Journal of Current Research in Engineering and Science
Bi-Annual Online Journal (ISSN: 2581 - 611X)
VOLUME:8, ISSUE:2, AUGUST 2025, PAPER NUMBER:45

Electrochemical Performance of Sodium Nickel Vanadium Phosphate mixed Polyanion Glass materials

Radhika G[1], Saritha Kumari Y[2], Nagamani G[3], and Sreekanth M[4]

[1,2,3] and [4] Faculty

Dept. of Humanities and Science,
Malla Reddy College of
Engineering, Hyderabad, India.

grandhe.radhika@gmail.com

Abstract: *The electrochemical impedance (EIS) performance of $NaNi_{1-x}(VO)_xPO_4$ (x=0.1, 0.3, and 0.5 mol%) mixed polyanion glass and glass-ceramic cathodes is correlated with structural stability in this work. $Na_4Ni_3(PO_4)_2(P_2O_7)$ (ICSD 82713), $NaNi_4(PO_4)_3$ (ICSD 60964), and NaV_2O_5 (ICSD 1898) crystalline phases are confirmed by XRD results. These phases are indexed with orthorhombic/Pna21, orthorhombic/Cmcm, and orthorhombic/Pmn21 structures, respectively. The highest conducting $NaNi_{0.7}(VO)_{0.3}PO_4$ glass-ceramic sample using a half-cell had the lowest charge-transfer resistance according to the inversion correlation between R_{ct} and $_b$. The glass-ceramic network $NaNi_{0.7}(VO)_{0.3}PO_4$ verifies that the current mixed polyanion glass-ceramic network has relatively flexible active centres in addition to its superior stability, which is what allows it to achieve the superior electrochemical performance.*

Keywords: *Glass Ceramic Cathode, crystalline phases, polyanion.*

1. Introduction

Due in large part to its high energy density and superior electrochemical performance, lithium-ion battery (LIB) technology has so far proven commercially successful for the portable electronics market as well as for electrical vehicles (EVs) [1, 2]. But when it comes to storing large amounts of energy, like solar and wind power, where cost is a major consideration and footprint can be compromised, LIB is not the first option . Because sodium-ion battery (SIB) technology and lithium-ion battery (LIB) technology operate on similar principles, [3, 4]. In the last five years or so, a great deal of research has been conducted on sodium-ion battery (SIB) technology in order to meet the demand for smart electric-Grid energy storage in the future [5, 6]. Despite the fact that there are n't many effective cathode and anode component systems for LIB technology, the following factors

prevent them from being directly transferred to SIB technology: i) Lower specific gravimetric capacity than Li metal (Na: 1165 mAh/g and Li: 3829 mAh/g), ii) heavier atomic size of Na' (~50 times heavier than Li) influences the stability of structural network during redox reaction, and, of course, iii) lower energy density. In very recent years, excellent results have been reported for a range of crystalline anode and cathode materials [7].All material networks, however, face problems with inadequate capacity, subpar cycle performance, lower practical energy density, and rate capability, which significantly restricts commercialization [8, 9]. In contrast to crystalline electrode networks, our group has been working on a variety of amorphous-based glass and glass-ceramic cathode networks that can provide good capacity retention and rate performance. This success has motivated us to gather additional information to assess Electrochemical Impedance Spectroscopy (EIS) studies along these lines . The collective findings of these studies demonstrate that glass and glass-ceramic cathodes have distinct benefits, such as greater practical capacity and reduced cost, but they also present certain obstacles, such as ionic and electronic conductivity, cycle capacity degradation, and thermal instability, which need to be addressed before ambient Na-ion batteries can be realised[10]. To tackle these concerns, we have examined the safety, appropriateness, and efficacy of $NaNi_{1-x}(VO)_xPO_4$ (x=0.1, 0.3, and 0.5) mixed polyanion glass and glass-ceramic cathodes in this paper, considering the following details for ambient Na-ion battery applications: i) The stability of the glass network would increase if transition metal oxides, like vanadium, were present because they could prevent structural degradation. ii) The size difference between the Ni^{2+} (0.69 Å) and Na^{+} (1.03 Å) ions is expected to prevent the glass network structure from degrading during sodiation and de-sodiation processes, allowing the capacity to be maintained even for longer periods of time; iii) When the Ni^{2+} ions enter the Vanadium-Phosphate glass network, the width of the activation barrier decreases, which promotes the migration of Na^{+} ions more than before, which is a crucial characteristic to claim better cycle stability [11]. By acting as pillar ions and preventing the collapse of the pyrophosphate structure, Ni^{2+} ions are the most advantageous cations in mixed polyanion-based sodium vanadate phosphate glass and glass-ceramic networks. Through surface reconstruction, structural and thermal stability, and energy density preservation, this will undoubtedly favour the delivery of higher discharge capacities even at lower potential[12]. Actually, the aim of this current work is precisely this broad and audacious goal.

2. Experimental Methodology

2.1. Materials Preparation

Using the melt-quench method, glass samples with a nominal composition of $NaNi_{1-x}(VO)_xPO_4$ (x=0.1, 0.3, and 0.5 mol%) were created. To create a homogenous mixture, A.R. grade Na2CO3, NiO, V2O5, and $(NH_4)_2PO_4$ were thoroughly mixed and ground in an agate mortar for 30 minutes. The well-combined raw materials were transferred to a covered alumina crucible and melted in an electric furnace for an hour at 1000°C. The resulting melts were then cooled on a brass plate and formed into glass by rolling them with a copper roller yield. Additionally, the homogenous nano scaled glass powders were created over the course of 30 hours using the high-energy ball milling method[13, 14]. The glass-

ceramics of the precursor glass samples were created by heating the precursor glasses for five hours at their respective crystallization temperatures (T_c) in a tubular electric furnace with a 5% H2-95% Ar atmosphere. Using a PAN analytical Diffractometer B.V equipped with a Cu target and a Ni filter operating at 40 kV and 30 mA (2h range), the crystallization phase details were examined using the XRD method. In a planetary ball mill with a 1:10 ball ratio, all glass-ceramic compounds were coated with 7wt% reduced graphene oxide for 30 minutes at 300 rpm.[15, 16]

2.2. Working Electrode Preparation

The 2032 half cell was designed with glass-ceramic nanoscaled powder as the active material, sodium metal foil as the counter electrode, and 1M $NaClO_4$ in a solution of ethylene carbonate (EC) and diethyl carbonate (1% V/V) as the electrolyte in order to analyze the electrochemical properties. The glass microfiber filter paper (Grade GF/F) from Whatman® is used to separate the electrode and electrolyte. With 85% active material, 5% polyvinylidene fluoride (PVDF), and 10% conductive carbon black, the glass-ceramic cathodic half-cell is a fictional device. There were about 3 mg of active material loaded onto the working electrodes. An N-methylepyroliden (NMP) slurry mixture was prepared. After homogenisation, the slurry was coated on thin aluminium foil and dried in a vacuum oven for ten hours at 90°C [17, 18] . An Admiral Squidstat Plus workstation (0.01-4 V; 100 KHz-0.1Hz) was used for all electrochemical investigations (CV, Impedance, Galvanostatic). Using a multichannel NEWARE battery tester, life cycle analysis of half-cell tests up to 1000 cycles at various C-rates is carried out. A multichannel battery test unit from Maccor, Inc., model 2000, is used in conjunction with a battery test unit model 1470, FRA model 1255 from Solartron, Inc. (Corrware and ZPlot software, Scribner Associates), and a potential window ranging from 0.001 to 4 V. The scan rate is 0.1 mV s^{-1}.

3. Results and Discussion

3.1. XRD studies

An example of this amorphous nature can be seen in the mixed polyanion $NaNi_{0.9}(VO)_{0.1}PO_4$ glass cathode sample's SEM image, which shows plane surface morphology in the image of XRD. But all of the samples are showing the same thing [Inset of Fig. 1]. All of the mixed polyanion $NaNi_{1-x}(VO)_xPO_4$ glass cathode samples crystallized at its T_c (glass-ceramic) have XRD patterns that indicate the phase formation and local structure (Fig. 1). The formation of conducting $Na_4Ni_3(PO_4)_2P_2O_7$ (ICSD 82713) and $NaNi_4(PO_4)_3$ (ICSD 60964) crystalline phases, with orthorhombic/P n a 21 and orthorhombic/C m c m structures, respectively, which are recognised as the most stable structures, is primarily responsible for the diffraction patterns that were seen here [19, 20]. Furthermore, Fig. 1 shows additional phases, such as $NaNi(PO_3)_3$ and NaV_2O_5, which are impure phases with an orthorhombic/P m n 21 structure. Fig 1 clearly shows that the tendency for the glass samples to crystallize during heat treatment increases as x increases, reaching 0.3 mol% ($NaNi_{0.7}(VO)_{0.3}PO_4$). It's also intriguing to note that Fig. 1 shows that the

partial substitution of tetrahedral VO_4 sites for NiO_6 structural sites in the glass-ceramic network, which shortens phosphate chains, is a major cause of the intensity variation of diffraction peaks[21]. This could play a significant part in enhancing the samples overall electrochemical performance.

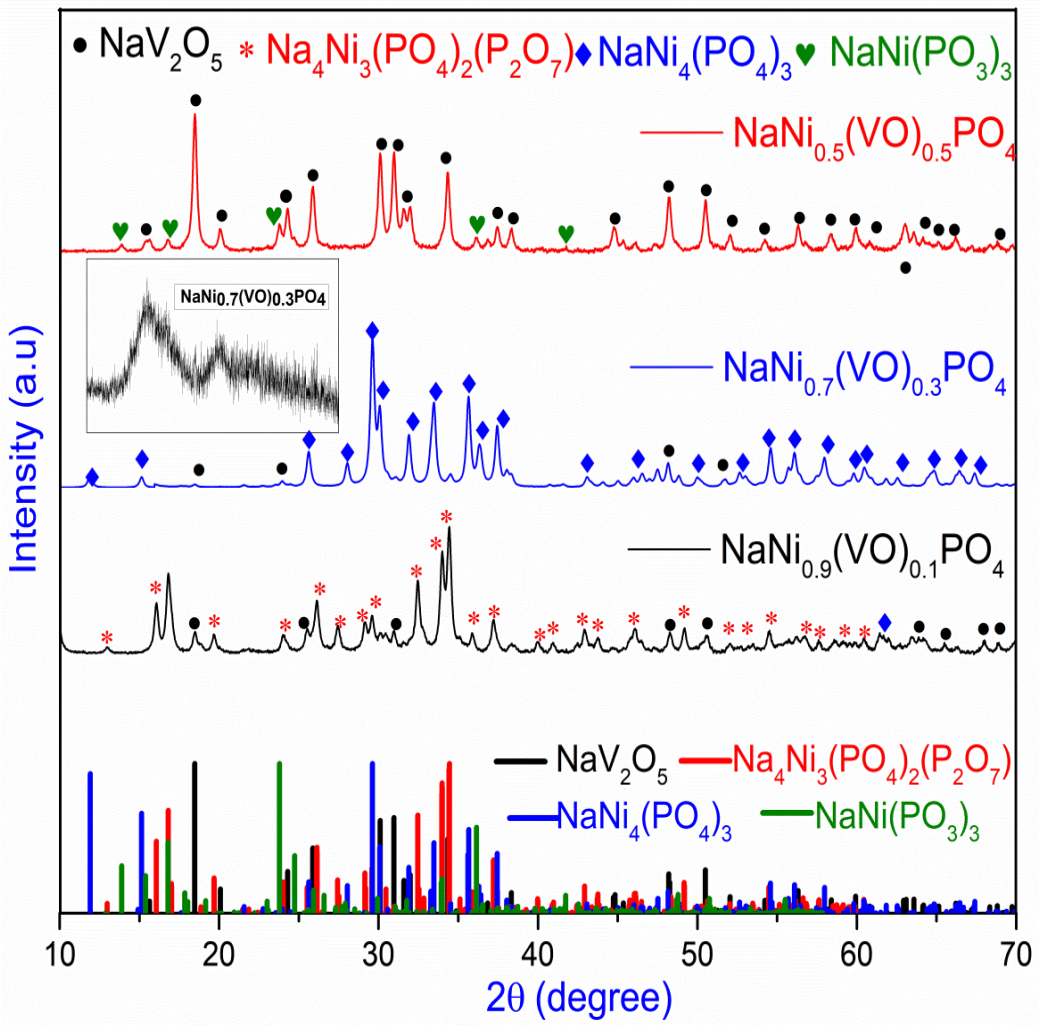

Fig. 1. XRD profiles of all $NaNi_{1-x}(VO)_xPO_4$ (x=0.1, 0.3, 0.5 mol%) glass-ceramic samples (inset shows $NaNi_7(VO)_3PO_4$ glass samples)

Table 1 Calculated and experimental structural parameters of mixed polyanion glass-ceramic cathode $NaNi_{1-x(}VO)_xPO_4$ (x=0.1, 0.3 and 0.5 mol %)

Mixed Polyanion glass-ceramic cathode composition $NaNi_{1-x(}VO)_xPO_4$ (x=0.1, 0.3 and 0.5 mol %)	Major Crystalline phase		Ref	a (Å)	b (Å)	c (Å)	α (°)	β (°)	γ (°)	Volume [Å^3]	Crystallite Size [nm]	Crystallization (%)	Crystal system/ Space group
$NaNi_{0.9(}VO)_{0.1}PO_4$	$Na_4Ni_3(PO_4)_2(P_2O_7)$	Exp.	1	18.0130	10.4110	6.4960	90	90	90	1218.22	78.1	74.25	Orthorhombic /P n a 21
		Cal.	This work	18.01(1)	10.418(8)	6.495(5)	90	90	90	1218.62			
		Δ(±)		0.003	0.007	0.001	0	0	0	0.4			
$NaNi_{0.7(}VO)_{0.3}PO_4$	$NaNi_4(PO_4)_3$	Exp.	2	6.3580	14.8420	9.8920	90	90	90	933.46	68.5	80.42	Orthorhombic / C m c m
		Cal.	This work	6.359(1)	14.846(2)	9.888(2)	90	90	90	933.53			
		Δ(±)		0.001	0.004	0.004	0	0	0	0.07			
$NaNi_{0.5(}VO)_{0.5}PO_4$	NaV_2O_5	Exp.	3	3.6110	4.7970	11.3180	90	90	90	196.05	100.4	87.63	Orthorhombic / P m n 21
		Cal.	This work	3.610(3)	4.802(4)	11.32(1)	90	90	90	196.32			
		Δ(±)	0.001	0.005	0.002	0	0	0	0.27	0.001			

3.2. Transport properties

An EIS study was conducted to estimate the electrochemical transport of Na^+ ions in the mixed polyanion $NaNi_{1-x}(VO)_xPO_4$ glass-ceramic cathode network. The study measured the voltage at room temperature (±10 mV) and the frequency range was 0.1Hz-10^6 MHz. A semicircle from the high to mid frequency domains and an inclined line over the low-frequency domain are used to depict nyquist plots (Fig. 2). For every $NaNi_{1-x}(VO)_xPO_4$ glass-ceramic sample, bulk resistance (R_b) was calculated using an intercept of the Z_{real} axis along the high-frequency portion of the semicircle[22, 23]. Charge-transfer resistance (R_{ct}) across the electrode/electrolyte interface is demonstrated by the semicircle's mid-frequency region (Table 2). Nonetheless, the solid electrode's diffusion of Na^+ ions is revealed by the low-frequency incline line. The area of contact and thickness of each glass and glass-ceramic sample are taken into account when calculating the bulk conductivity (σ_b) ($\sigma_b = (t/A)*(1/R)$). The charge transfer resistance (R_{ct}) and electrical conductivity (σ_b) as a function of composition are shown in the inset of Fig 2. The lowest perceived charge-transfer resistance ($R_{ct} = 7.2x10^3\Omega$) for the highest-conducting $NaNi_{0.7}(VO)_{0.3}PO_4$ glass-ceramic sample ($\sigma_b = 1.38x10^{-3}$ S/cm) was observed in the inversion correlation between R_{ct} and σ_b (Table 2 and Fig. 2). Furthermore, it is crucial to understand that the limitations in the Na^+ ion diffusion during insertion or removal are the reason why the R_{ct} values are increasing, usually with an increase in vanadium content from 0.1 to 0.3 mol%. Hence, it is clearly predicted that the stable Orthorhombic /P n a 21 ($Na_4Ni_3(PO_4)_2(P_2O_7)$, and Orthorhombic/ C m c m ($NaNi_4(PO_4)_3$ phase) structures coupled with higher electrical conductivity would trigger Na^+ ion diffusion leading to boost the electron movement in the $NaNi_{0.7}(VO)_{0.3}PO_4$ glass–ceramic network (Fig 3). Additionally, As will be discussed in the next section, the flexibility of the active centres allows them to easily accept the Na^+ ion, which activates the intercalation/de-intercalation via this glass-ceramic network and affects the cycle performance and charge capacity.

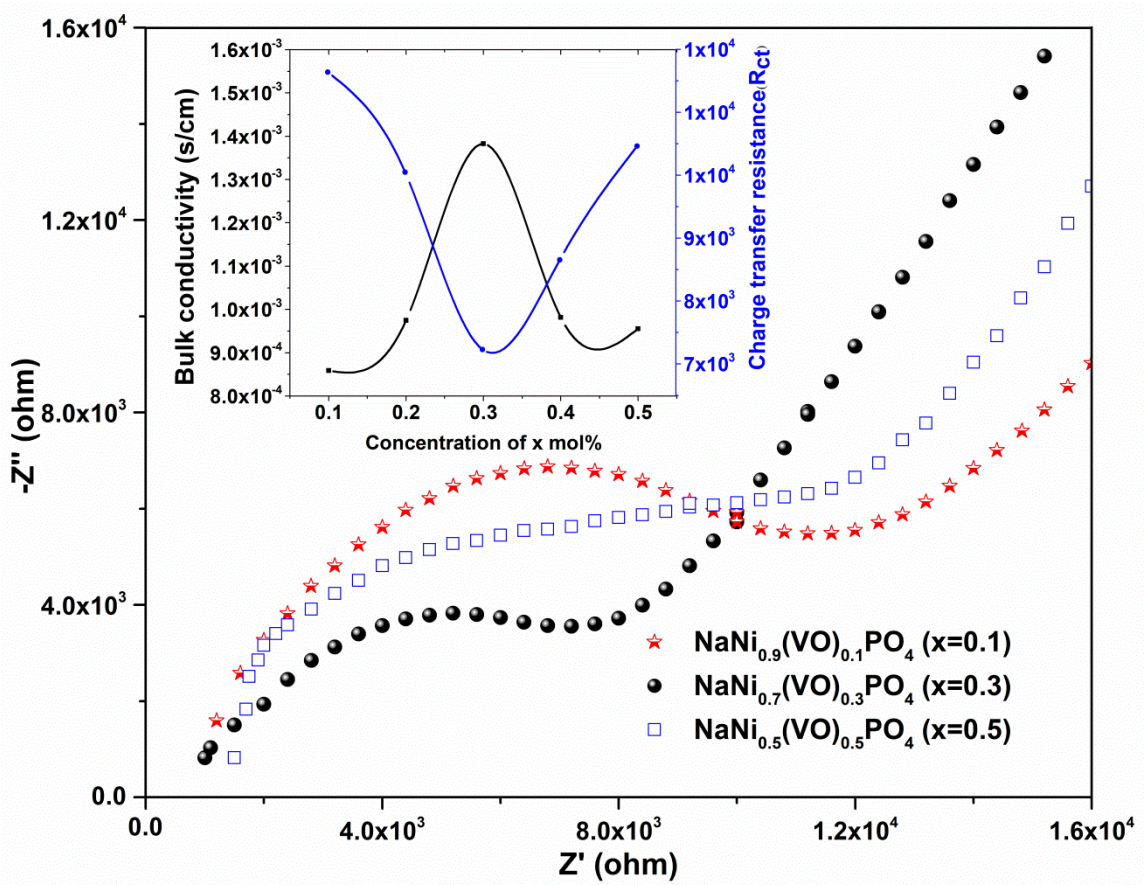

Fig. 2. EIS spectroscopy of all $NaNi_{1-x}(VO)_xPO_4$ (x=0.1, 0.3, 0.5 mol%) glass-ceramic samples.

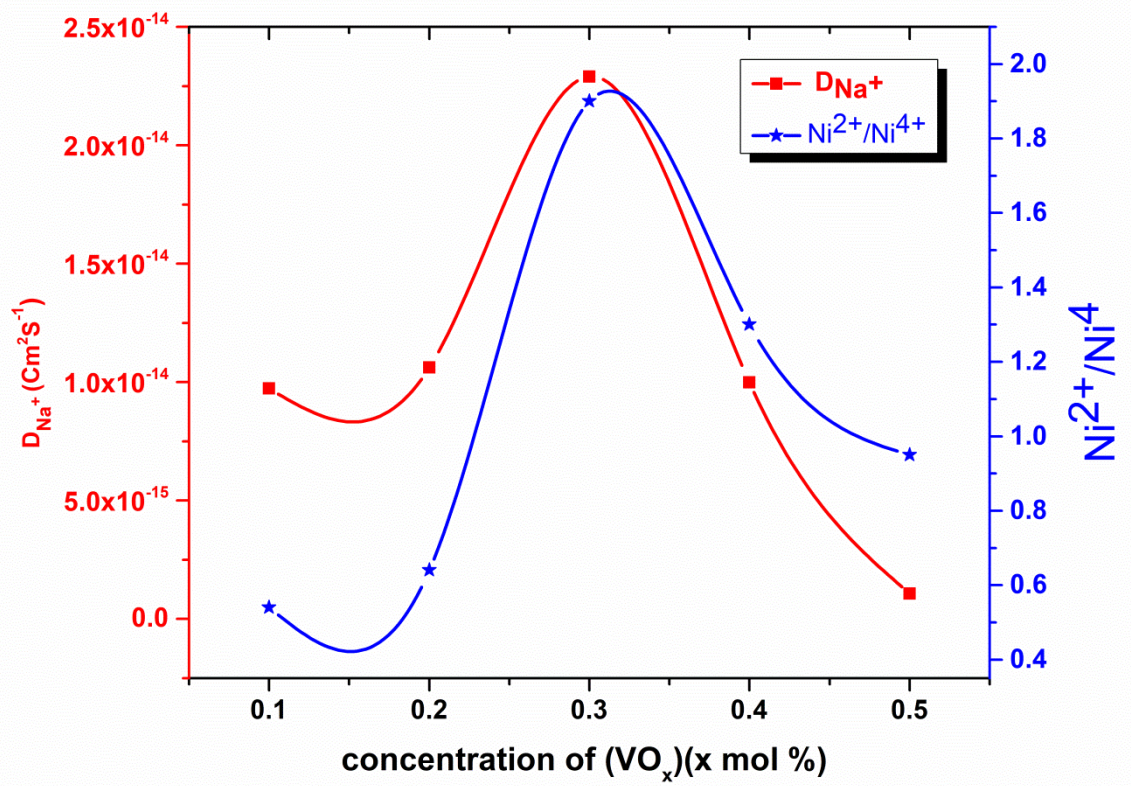

Fig. 3. Correlation between the Ni^{4+}/Ni^{2+} ratio and the diffusion coefficient of Na-ion (D_{Na+}) against composition

Table 2 The crystallization and the average grain sizes of the of all mixed polyanion glass-ceramic cathode.

Mixed polyanion glass-ceramic cathode	Charge transfer resistance (R_{ct})	Conductivity (σ_{dc}) S/Cm	$D_{Na^+}(Cm^2S^{-1})$	Anodic Voltage (V)	Cathodic Voltage (V)	Polarization (V)
$NaNi_{0.9}(VO)_{0.1}PO_4$	1.16 $x10^4$	8.5917 $x10^{-04}$	9.7302 $x10^{-15}$	2.1	1.68	0.42
$NaNi_{0.7}(VO)_{0.3}PO_4$	7.22 $x10^3$	1.38$x10^{-3}$	2.2902 $x10^{-14}$	2.18	1.82	0.36

$NaNi_{0.5}(VO)_{0.5}PO_4$	1.04 $x10^4$	9.5546 $x10^{-4}$	1.0663 $x10^{-15}$	2.35	1.88	0.47

3.5. Electrochemical analysis

For any material network, the EIS is an essential tool for tracking the redox reaction during the charge and discharge process. Fig 4 shows the charge and discharge profiles of the mixed polyanion $NaNi_{1-x}(VO)_xPO_4$ glass-ceramic cathode network at 0.1C. The charge and discharge profiles all clearly show a sloping plateau region between (1.8 - 3.0 V), which allows for the insertion or removal of Na^+ ions via the glass-ceramic network in various directions (Fig 4a–c). For every glass-ceramic cathode sample, the first discharge and charge capacities are 69.8, 86.2, 66 mAh/g and 54.5, 79.3, 60.4 mAh/g, respectively, when measured at 0.1 C. The 20^{th} cycles discharge and charge capacities are, correspondingly, 56.2, 82.3, 63 mAh/g and 42.1, 78.3, 51.2 mAh/g. This pattern will shorten the electron migrations path, accelerating the diffusion of Na^+ ions and restoring the redox reaction's equilibrium [24].

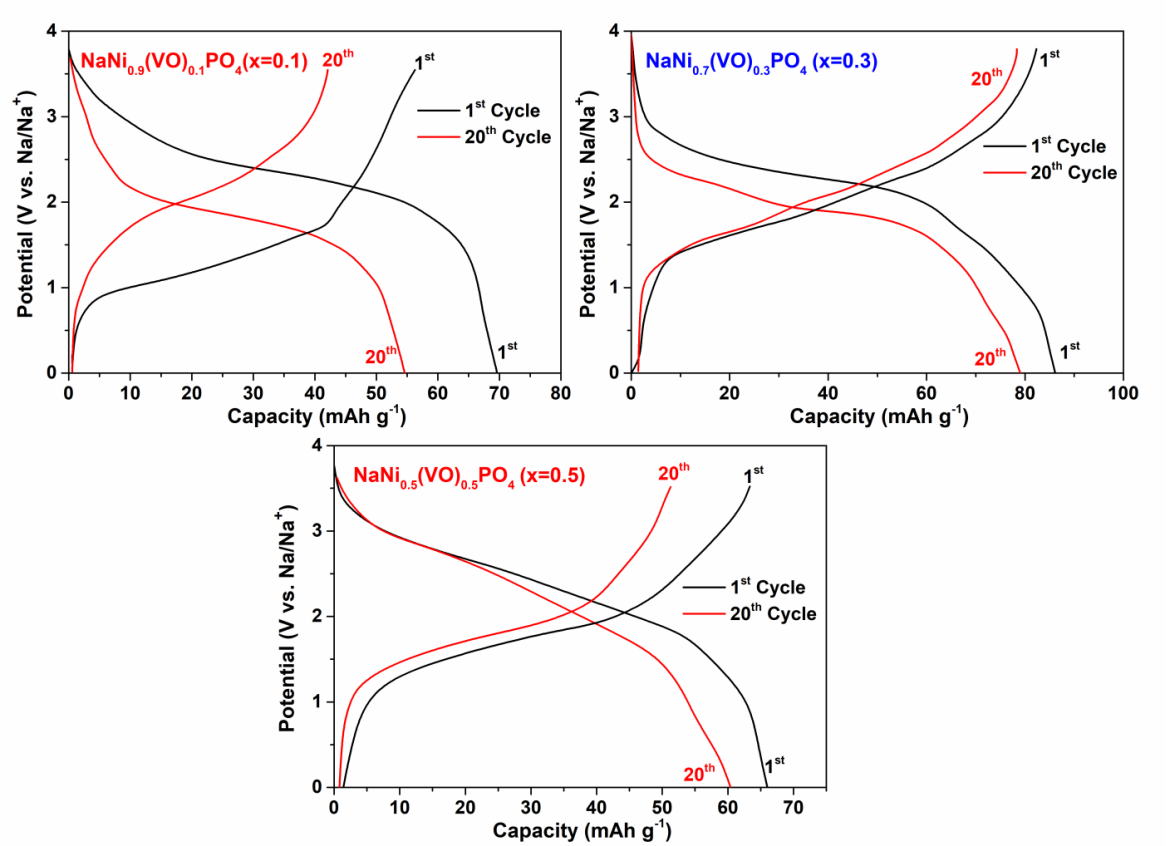

Fig. 4. Charge and discharge profiles for 1^{st} and 20^{th} cycles of all $NaNi_{1-x}(VO)_xPO_4$ (x=0.1, 0.3, 0.5 mol%) glass-ceramic samples measured at 0.1 C rate.

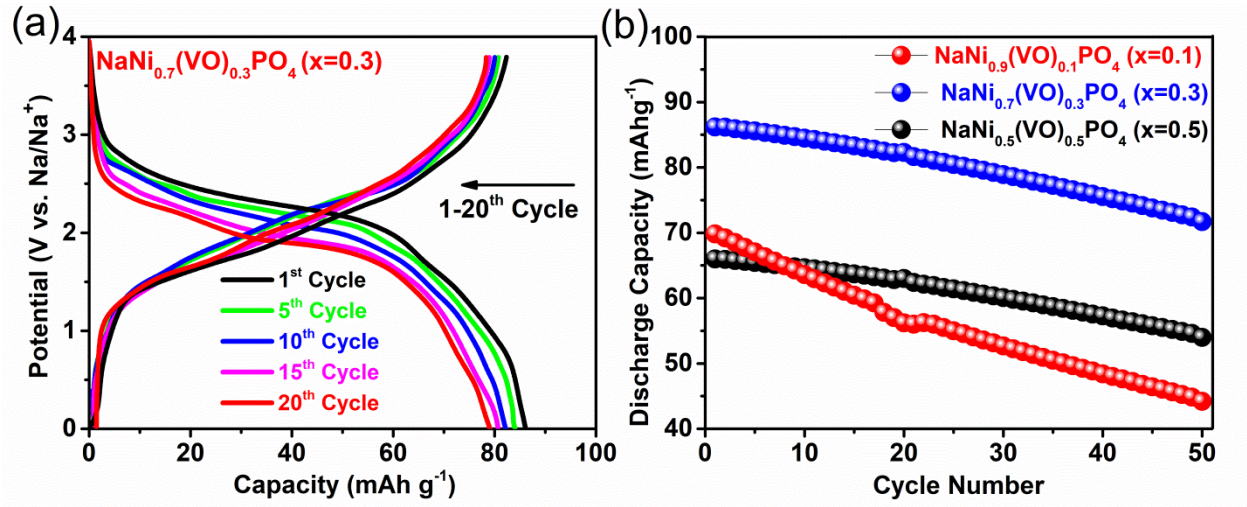

Fig. 5. a) Charge and discharge profiles of the best conducting glass-ceramic sample ($NaNi_{0.7}(VO)_{0.3}PO_4$) samples measured at a rate of 0.1C. (b) Discharge capacities of all the $NaNi_{1-x}(VO)_xPO_4$ (x=0.1, 0.3, 0.5 mol%) glass-ceramic samples measured at a rate of 0.1C up to 100 cycles.

Table 3. Summary of charge/discharge capacity and reversible efficiency of all mixed polyanion glass-ceramic cathode

Mix polyanion glass-ceramic cathode	First discharge capacity (mAh g^{-1})	First charge capacity (mAh g^{-1})	Capacity loss in the first cycle (mAh g^{-1})	Reversible efficiency in the first cycle (%)	Discharge capacity at 20^{th} cycle (mAh g^{-1})	Charge capacity at 20^{th} cycle (mAh g^{-1})	Capacity loss after 20 cycles (mAh g^{-1})	Reversible efficiency for 20 cycles (%)
$NaNi_{0.9}(VO)_{0.1}PO_4$	69.8	54.5	15.3	78	56.2	42.1	14.2	74.7
$NaNi_{0.7}(VO)_{0.3}PO_4$	86.2	79.3	6.9	92	82.3	78.3	4	95.13
$NaNi_{0.5}(VO)_{0.5}PO_4$	66	60.4	5.6	91.5	63	51.2	14.8	81.2

Table 4. Summary of discharge capacity and ionic conductivity of all mixed polyanion glass-ceramic cathodes.

Mixed polyanion glass-ceramic cathode	Theo. discharge capacity (mAh g^{-1})	Exp. Discharge capacity (mAh g^{-1})						Conductivity (σ_{dc}) S Cm^{-1}
		1^{st} cycle	50^{th}	Discharge capacity retention %	1^{st} cycle 0.1C	50^{st} cycle 10C	Discharge capacity retention %	

		(0.1C rate)	cycle (0.1C rate)		rate	rate		
$NaNi_{0.9}(VO)_{0.1}PO_4$	151	69.8	44.2	63.32	69.8	41	58.73	568E-07
$NaNi_{0.7}(VO)_{0.3}PO_4$	149.6	86.2	71.7	83.17	86.2	69	80.04	8.84E-07
$NaNi_{0.5}(VO)_{0.5}PO_4$	148.2	66	54	81.81	66	44	66.66	6.63E-07

The optimal-conducting glass-ceramic cathode sample's discharge and charge capacities, which were determined to be 86.2 $mAhg^{-1}$, 79.3 $mAhg^{-1}$ and 82.3 $mAhg^{-1}$, 78.3 mAh/g for the first and twentieth cycles, respectively, also seemed to be near to their theoretical capacity. One important feature of this network family is that the loss in discharge capacity is very small (4 mAh/g) within this range (Fig. 5a). The best conducting glass-ceramic cathode network's four-channel migration pathways of Na^+ ions through the $Na_4Ni_3(PO_4)_2(P_2O_7)$ and $NaNi_4(PO_4)_3$ phases are anticipated to shorten electron paths, improving electronic conductivity [25]. On the other hand, as shown in Fig. 5b, it is equally important to keep an eye on the discharge capacity profile for each sample of the $NaNi_{1-x}(VO)_xPO_4$ glass-ceramic network up to 50 cycles (0.1C). It is important to note that the sample with the highest conductivity ($NaNi_{0.7}(VO)_{0.3}PO_4$) produced good capacity retention (83.17%) and an excellent discharge capacity, both of which are critical for use in large-scale energy storage devices (Table 4). The best $NaNi_{0.7}(VO)_{0.3}PO_4$ glass-ceramic sample shows a progressive decrease in discharge capacity from 0.1 C to 10 C rates in Fig. 6a, illustrating the change in discharge capacity against variable current rates. This trend is observed for all the samples that are being investigated. Similarly, Fig. 6b shows the cycle life dependent rate capability for each glass-ceramic cathode sample as a function of current rates. Additionally, it is once more demonstrated that the highest discharge capacity retention (80.04%) is comparatively delivered by the best-conducting glass-ceramic sample ($NaNi_{0.7}(VO)_{0.3}PO_4$) (Table 6), The best conducting $NaNi_{0.7}(VO)_{0.3}PO_4$ glass-ceramic cathode network may have a higher concentration of NiO_6 octahedral structural units at higher current rates (10C), which could lead to the formation of distinct Na^+ ion migration pathways via the $Na_4Ni_3(PO_4)_2(P_2O_7)$ and $NaNi_4(PO_4)_3$ phases. This would undoubtedly improve the electrochemical performance to a greater extent, as suggested by computational diffusion pathways analysis. However, when the current rate returns to 0.1C from 10C, good capacity retention is seen, which unquestionably increases the cycle life stability and rate capability compared to other crystalline compounds. However, the degree of purity in the redox reaction from lower (0.1C) to higher current rates (10C) may be directly related to the poor electrical conductivity for the remaining glass-ceramic cathode samples.

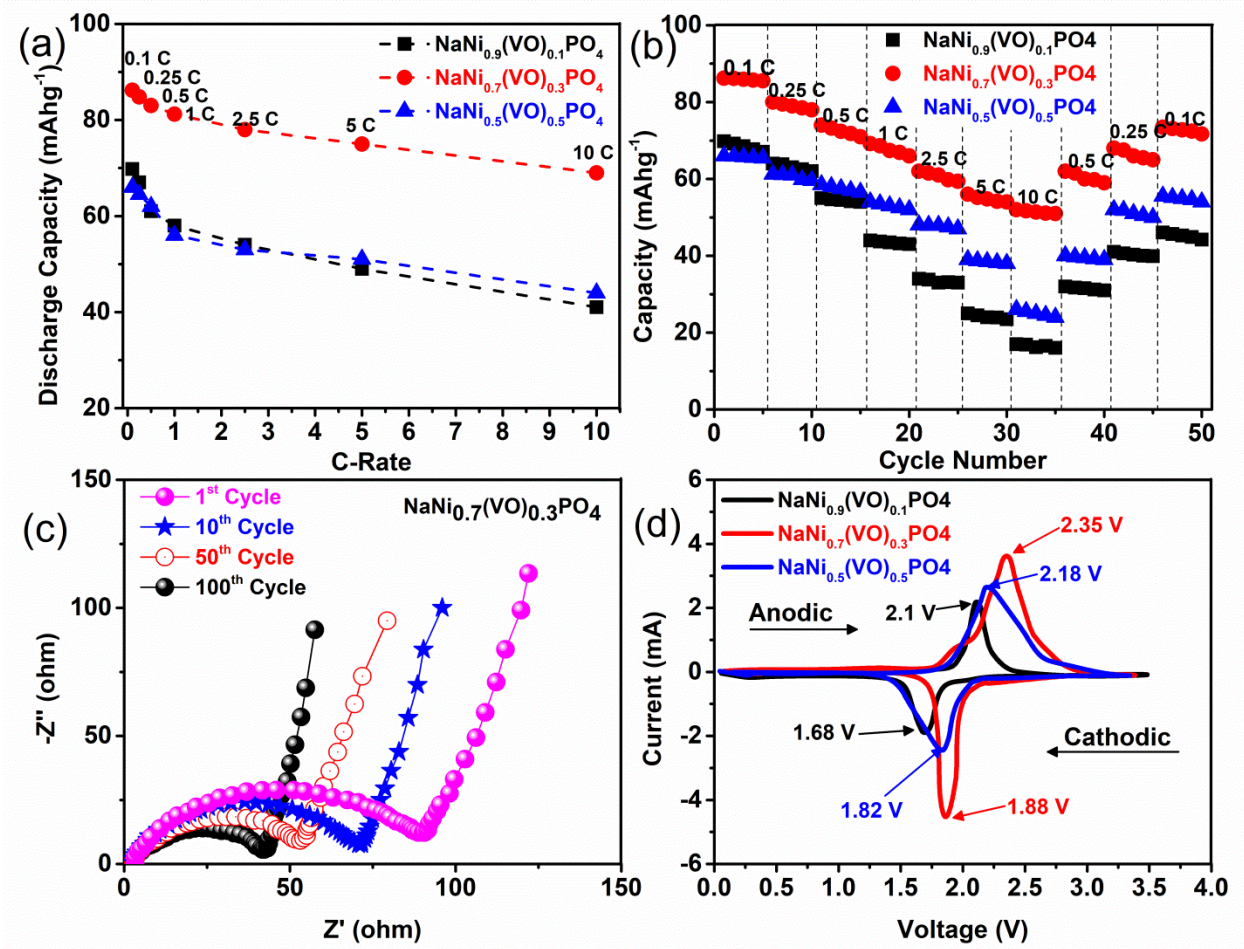

Fig. 6. (a) Discharge capacities of all the $NaNi_{1-x}(VO)_xPO_4$ (x=0.1, 0.3, 0.5 mol%) glass-ceramic samples measured at 0.1C, 0.25C, 0.5C, 1C, 5C, and 10C. (b) Rate capabilities of all the $NaNi_{1-x}(VO)_xPO_4$ (x=0.1, 0.3, 0.5 mol%) glass-ceramic samples measured at different C-rates up to 50 cycles. (c) EIS of the best-conducting glass-ceramic sample ($NaNi_{0.7}(VO)_{0.3}PO_4$) sample after 1, 10, 50 and 150 cycles measured at a rate of 0.1C.(d) Cyclic voltammogram of all the $NaNi_{1-x}(VO)_xPO_4$ (x=0.1, 0.3, 0.5 mol%) glass-ceramic samples measured at a rate of 0.1C.

When measured at 0.1C, the Nyquist curves in Fig. 6c for the best conducting sample show a single semicircle at its middle frequency range, followed by a spike even up to 100 cycles. To determine the minimum charge transfer resistance (R_{ct}) for the optimal $NaNi_{0.7}(VO)_{0.3}PO_4$ glass-ceramic cathode-network cathode composition, utilize the diameter of semicircles in Fig 6c. To record the cyclic voltammogram of $NaNi_{1-x}(VO)_xPO_4$ half-cells over voltage between 0.5 - 4 V at 100 µV/s, Fig. 6d is provided. Note-down cell polarization is directly caused by the difference between the oxidation (2.35, 2.18, 2.1 V) and reduction (1.88, 1.82, 1.68 V) peak positions[26]. Because of its greatest cycle-life ability and easy Na^+ ion diffusion migration, the best-conducting $NaNi_{0.7}(VO)_{0.3}PO_4$ glass-ceramic network in this instance showed the least amount of polarization[27]. (Table 2).

4. Conclusions

As the most stable structures, conducting $Na_4Ni_3(PO_4)_2(P_2O_7)$ and $NaNi_4(PO_4)_3$ crystalline phases with orthorhombic/P n a 21 and orthorhombic/C m c m structures, respectively, were the most frequently formed, according to XRD patterns. Nyquist plots revealed that, as expected given the precipitation of stable Orthorhombic /P n a 21 and Orthorhombic /C m c m structures during the conversion of glass into glass-ceramic network, higher electrical conductivity ($1.38x10^{-3}$ S/cm) and lowest R_{ct} would cause Na^+ ion diffusion, leading to boost the electron movement in the $NaNi_{0.7}(VO)_{0.3}PO_4$ glass-ceramic network. Because of its thin particle-electrolyte interface, which causes Na+ ion diffusion to migrate, the best-conducting $NaNi_{0.7}(VO)_{0.3}PO_4$ glass-ceramic network has the lowest polarization value, the highest cycle life ability, discharge and charge capacity (82.3, 78.3 mAh/g), and superior reversible efficiency (95.13%). Mixed polyanion $NaNi_{1-x}(VO)_xPO_4$ glass-ceramic cathode networks superior structural stability and EIS properties make it stand out as a potentially promising cathode component for "Smart-Grid" storage applications. However, more validation work is needed for industrial scale-up and reliable life-cycle performance under commercial conditions.

References:

[1] S. S. Rangarajan, S.P. Sunddararaj, A. Sudhakar, C.K. Shiva, U. Subramaniam, E.R. Collins, T. Senjyu, Lithium-ion batteries.The crux of electric vehicles with opportunities and challenges, Clean Technologies, 4 (2022) 908-930.

[2] X. Zeng, M. Li, D. Abd El-Hady, W. Alshitari, A.S. Al-Bogami, J. Lu, K. Amine, Commercialization of lithium battery technologies for electric vehicles, Advanced Energy Materials, 9 (2019) 1900161.

[3] W. Zhang, J. Lu, Z. Guo, Challenges and future perspectives on sodium and potassium ion batteries for grid-scale energy storage, Materials Today, 50 (2021) 400-417.

[4] R. Rajagopalan, Y. Tang, X. Ji, C. Jia, H. Wang, Advancements and challenges in potassium ion batteries: a comprehensive review, Advanced Functional Materials, 30 (2020) 1909486.

[5] J. Zhang, T. Liu, X. Cheng, M. Xia, R. Zheng, N. Peng, H. Yu, M. Shui, J. Shu, Development status and future prospect of non-aqueous potassium ion batteries for large scale energy storage, Nano Energy, 60 (2019) 340-361.

[6] L.P. Wang, L. Yu, X. Wang, M. Srinivasan, Z.J. Xu, Recent developments in electrode materials for sodium-ion batteries, Journal of Materials Chemistry A, 3 (2015) 9353-9378.

[7] A. Eftekhari, D.-W. Kim, Sodium-ion batteries: new opportunities beyond energy storage by lithium, Journal of Power Sources, 395 (2018) 336-348.

[8] V.K. Tiwari, R.K. Singh, Nanostructured coating strategies of cathode for improved sodium ion battery performance, Chemical Engineering Journal, 471 (2023) 144592.

[9] N. Tapia-Ruiz, A.R. Armstrong, H. Alptekin, M.A. Amores, H. Au, J. Barker, R. Boston, W.R. Brant, J.M. Brittain, Y. Chen, 2021 roadmap for sodium-ion batteries, Journal of Physics: Energy, 3 (2021) 031503.

[10] S. Mariyappan, Q. Wang, J.M. Tarascon, Will sodium layered oxides ever be competitive for sodium ion battery applications?, Journal of The Electrochemical Society, 165 (2018) A3714.

[11] Y. Li, L. Zhang, X. Wang, X. Xia, D. Xie, C. Gu, J. Tu, High capacity and superior rate performances coexisting in carbon-based sodium-ion battery anode, Research, (2019).

[12] S. Gandi, S.R. Chinta, P.K. Ojha, M.S. Surendra Babu, B.R. Ravuri, High Na-ion conducting Na1+ x [SnxGe2− x (PO 4) 3] glass-ceramic electrolytes: Structural and electrochemical impedance studies, Journal of the American Ceramic Society, 101 (2018) 167-177.

[13] G. Huang, C. Lv, J. He, X. Zhang, C. Zhou, P. Yang, Y. Tan, H. Huang, Study on preparation and characterization of graphene based on ball milling method, Journal of Nanomaterials, 2020 (2020) 2042316.
[14] M. Naghdi, M. Taheran, S.K. Brar, T. Rouissi, M. Verma, R.Y. Surampalli, J.R. Valero, A green method for production of nanobiochar by ball milling-optimization and characterization, Journal of Cleaner Production, 164 (2017) 1394-1405.
[15] S. Fatimah, R. Ragadhita, D.F. Al Husaeni, A.B.D. Nandiyanto, How to calculate crystallite size from x-ray diffraction (XRD) using Scherrer method, ASEAN Journal of Science and Engineering, 2 (2022) 65-76.
[16] H. Khan, A.S. Yerramilli, A. D'Oliveira, T.L. Alford, D.C. Boffito, G.S. Patience, Experimental methods in chemical engineering: X-ray diffraction spectroscopy—XRD, The Canadian journal of chemical engineering, 98 (2020) 1255-1266.
[17] R. Morasch, B. Suthar, H.A. Gasteiger, Simple way of making free-standing battery electrodes and their use in enabling half-cell impedance measurements via μ-reference electrode, Journal of The Electrochemical Society, 167 (2020) 100540.
[18] G. Yuan, G. Wang, H. Wang, J. Bai, Half-cell and full-cell investigations of 3D hierarchical MoS2/graphene composite on anode performance in lithium-ion batteries, Journal of Alloys and Compounds, 660 (2016) 62-72.
[19] A. Rapacz-Kmita, C. Paluszkiewicz, A. Ślósarczyk, Z. Paszkiewicz, FTIR and XRD investigations on the thermal stability of hydroxyapatite during hot pressing and pressureless sintering processes, Journal of Molecular Structure, 744 (2005) 653-656.
[20] B. Mandal, N. Garg, S.M. Sharma, A. Tyagi, Preparation, XRD and Raman spectroscopic studies on new compounds RE2Hf2O7 (RE= Dy, Ho, Er, Tm, Lu, Y): Pyrochlores or defect-fluorite?, Journal of Solid State Chemistry, 179 (2006) 1990-1994.
[21] A. Hashem, A. Abdel-Ghany, A. Eid, J. Trottier, K. Zaghib, A. Mauger, C. Julien, Study of the surface modification of LiNi1/3Co1/3Mn1/3O2 cathode material for lithium ion battery, Journal of Power Sources, 196 (2011) 8632-8637.
[22] X.-Z. Liao, Z.-F. Ma, Y.-S. He, X.-M. Zhang, L. Wang, Y. Jiang, Electrochemical behavior of LiFePO4∕C cathode material for rechargeable lithium batteries, Journal of the Electrochemical Society, 152 (2005) A1969.
[23] R. Grandhe, V.K. Katta, M.R. Padala, D.P. Dutta, WisanuPecharapa, B.R. Ravuri, PolyanionNaNi1−xCuxPO4 glass and glass-ceramic cathode network: Structure with improved electrochemical performance, Applied Physics A, 130 (2024) 470.
[24] V.K. Katta, S. Gandi, N.K. Katari, W. Mekprasart, W. Pecharapa, D.P. Dutta, B.R. Ravuri, Mixed polyanion Na-Mn-V-P glass–ceramic cathode network: improved electrochemical performance and stability, Energy Technology, 9 (2021) 2000845.
[25] S. Gandi, V.K. Katta, D.P. Dutta, B.R. Ravuri, A mixed polyanion NaFe 1− x (VO) x PO 4 glass-ceramic cathode system for safe and large-scale economic Na-ion battery applications, New Journal of Chemistry, 44 (2020) 2897-2906.
[26] V.K. Katta, N.K. Katari, D.P. Dutta, M.F. Mohd Sabri, B.R. Ravuri, Enhanced Long Cycle Life Stability and High Storage Reversible Capacity Retention of a Sodium Vanadate Zinc Glass–Ceramic Network, Energy & Fuels, 36 (2022) 6492-6501.
[27] S.K. Yerranuka, V.K. Katta, P. Ghosal, B.R. Ravuri, Sodium-Bismuth-Titanium glass–ceramic network: A high capacity anode network for Na+ ion storage, Journal of Non-Crystalline Solids, 621 (2023) 122609.